

Crossing, or bi-modal sea states occur between 5 and 40 % of the time in the North Sea (Guedes Soares, 1984). These are generated when swell waves propagating into the region from distant storm events interact with locally-generated waves which may be of very different direction, period and height. Swell waves from the North Atlantic and Norwegian Sea propagate into the North Sea, interacting with local windsea generated waves, modifying the main spectral parameters. The interaction between differing wave-trains is not fully understood, but crossing seas have been statistically associated with freak wave incidence, and shipping accidents (Waseda et al., 2011; Tamura et al., 2009; Cavaleri et al., 2012; Onorato et al., 2006, 2010; Sabatino and Serio, 2015; Toffoli et al., 2011). The North Sea is particularly prone to rogue wave events, such as the famous Draupner Wave recorded in 1994 (Haver, 2004), the first ever recorded rogue wave event, that occurred in crossing sea conditions (Adcock et al., 2011).

In addition to crossing seas, wave–current interactions are a well known cause of wave height amplification or attenuation. Wave–currents interactions (WCI) are depth- and current-induced modification of wave features. A seminal study carried out by Tolman (1991) highlighted that wave–current interactions are significant in the North Sea, changing the significant wave height (H_s) and the mean wave period (T_m) by 5 and 10 % respectively during storm periods. However the model that was used by Tolman (1991) to assess this effect, was at very coarse resolution and broad scale. In particular the effect of the WCI in the coastal shallow areas was not considered. Phillips (1977) showed that in the absence of wave-breaking, local wave amplitude is given by:

$$\frac{A}{A_0} = \frac{c_0}{\sqrt{c(c + 2U)}} \quad (1)$$

where A is the resulting wave amplitude, A_0 is the unperturbed amplitude of the wave field, c is the wave phase speed, and U is the current that interacts with the wave train. It is important to notice that the sign of the current is determinant on the effect of the WCI: if the current travels in opposite direction with the wave train, there will be an enhancement of the significant wave height. Conversely if current and waves are in the

3101

same direction, the H_s decreases. For deep water waves, the phase speed, c , depends only on the period of the wave, while in shallow water c depends only on the depth. Equation (1) shows that the waves travelling in a direction opposing the current ($U < 0$) have a positive ratio A/A_0 and, consequently, an enhancement of the wave amplitude.

Wave–current interactions could also lead to the breaking of the wave: if the current is strong enough to block the wave train (Ris and Holthuijsen, 1996), these waves can break and lose energy before arriving to the coastline (Chawla and Kirby, 2002, 1998).

WCI are particularly difficult to quantify empirically, and computationally intensive to model. However, it is clear that shallow coastal waters, embayments and headlands are particular foci for interactions (Hearn et al., 1987; Signell et al., 1990). Model studies have concentrated on comparing wave height and period in coupled and uncoupled model versions showing, for example, 3 % difference in wave height and 20 % in wave period in the Dutch and German coastal waters of the North Sea (Osuna and Monbaliu, 2004). Similar results have been obtained for coastal waters of the Adriatic during Bora conditions (Benetazzo et al., 2013), finding a maximum reduction for the H_s of 0.6 m in the central Adriatic and a simultaneous increase up to 0.5 m in Trieste and Venice Gulf. WCI were also studied during hurricane conditions off the eastern seaboard of the USA (Xie et al., 2008).

Sea defences of coastal settlements along the northeast coast of Scotland have suffered several damaging events during the period 2009–2014 as a result of surge and wave. The coastal waters are dominated by strong tidal currents and wind-driven residuals, and are exposed to wave trains entering the North Sea from the north, and generated by storm events in the central and southern North Sea. Although the oceanography of the North Sea as a whole has been intensively studied since the 1830s (Whewell, 1830; Proudman and Doodson, 1924; Dietrich, 1950; Huthnance, 1991; Otto et al., 1990), and the region was one of the earliest to be subjected to computational hydrodynamic modelling (Flather, 1987; Davies et al., 1985), high resolution modelling activity has been largely concentrated in areas with potential for wave and tidal energy extraction (Adcock et al., 2013; Bryden and Couch, 2006; Baston and

3102

coupled model was 0.97 s in Aberdeen, 1.24 s in the Firth of Forth and 1.83 s in the Moray Firth). Comparing satellite observations in spring and winter conditions, it is possible to conclude that, in general, the model provides accurate predictions for wave heights < 1.5–2 m, but slightly underestimates the height of larger waves. On the other hand, wave periods are better modelled in winter period, where the waves are higher. No or very small differences were recorded between coupled and uncoupled model for satellite validation. This because the resolution of the satellite data is low and because the satellite data are often in deep water, where the WCI are less important.

3.3 Wave–current interaction

Predicted wave field with and without wave–current interaction were compared during a 7 month period in 2010, covering both winter and summer conditions, for evaluating the importance of WCI on wave features. The results are shown in Fig. 4. For the comparison between the coupled and the uncoupled model the Root Mean Square (RMS) between the two runs was computed. Results show some differences between the two runs, in particular, the largest deviations, due to WCI, are found in coastal areas, such as around headlands, bays and in estuaries, in which the currents (mostly driven by tides) are strongest. As expected the highest differences were seen in the proximity of the coastline (Signell et al., 1990): this was because the strength of the currents (mainly tidal-driven) are stronger (Dietrich, 1950; Otto et al., 1990). During spring tides, higher values for the current were recorded off Northeast England and near Peterhead and Aberdeen (see Fig. 1). Wave periods are more affected than wave heights in this coupling, with RMS deviations that can be on average of 20 % (absolute value) in shallow-water coastal areas. We also considered the effect of the wave–current interactions on the wave directional spreading, as this is an important variable for the stability of the wave train in deep water and on its evolution (Benjamin and Feir, 1967). The results showed that during the 7 month period the significant wave height was, on average, less affected than directional spreading or wave periods: the difference was of the order of magnitude of 0.1 m near the coastline and less offshore, while the difference

3111

in peak spectral wave period (T_p) exceeded 1 s in some of the east coast Firths such as the Moray Firth and the Firth of Forth. The maximum variation of H_s between the coupled and the uncoupled run was +3 and –2 m, both occurring during storm events.

3.4 Current and swell effect on the wind-sea wave field

In order to study the importance of the wave–current interactions and the coupling between swell and wind-sea waves off the east coast of Scotland, three storms were considered in the period January–August 2010. Storm events were identified by examining the time series in the Firth of Forth and the Moray Firth in which the highest H_s were recorded. These three storms were selected because they were the three most intense storms during the considered period and originated from different weather conditions.

3.4.1 The 26–27 February 2010 storm

Between the 25–27 February 2010, the UK was affected by a low pressure system, that moved rapidly from west to east. From the afternoon of the 25th to the 26th the centre of the storm was over the North Sea (Fig. 5). At the same time, another low pressure system (not shown in the map) was over the Norwegian Sea, causing a train of swell moving from N to S. The low pressure over North Sea caused windsea waves exceeding 4 m. In Fig. 6 the situation in the sea is showed at 12:30 UTC of the 26th: swell waves contributed to enhancing the H_s in the centre of the storm, while a train of swell waves was forming from this storm, travelling west to the Moray Firth. Interaction of the windsea and the swell waves caused high waves along the east coast: the maximum recorded H_s by the Firth of Forth wave gauge was 4.8 m. WCI contributed to the enhancement of H_s by up to 1 m in coastal areas, while in the open sea the contribution was very low, up to 0.1 m. In the afternoon of the 26th (Fig. 7, at 19:00 p.m.) the storm was near the Firth of Forth. The contribution of the swell waves was significant, increasing the H_s by up to 1 m: model outputs showed that the central part of the storm had a $H_s > 5$ m, while without the swell coming from North the centre of the storm would

3112

have been an $H_s < 4.5$ m. To our knowledge no significant damages were recorded for this storm.

3.4.2 The 30–31 March 2010 storm

The larger storm in 2010 occurred during the night of 30 March 2010. Between 29 March 2010 and 1 April 2010 the SE coast of Scotland and the north of England was struck by severe weather and very strong winds. These conditions were caused by a strong depression that originated from a weak minimum near the Azores Islands, in the North Atlantic, in front of the Portuguese coast. This low pressure was < 990 hPa once over Great Britain and Ireland at midnight of the 30 March 2010 and reached its minimum the day after with a depression of < 980 hPa over the North of England. The evolution of the storm from surface pressure charts from ECMWF ERA-Interim reanalysis is reported in Fig. 8 (Dee et al., 2011; Berrisford et al., 2011). These figures clearly show that the depression, at its maximum strength, is just above the S of Scotland during the night between the 30–31 March 2010. This depression generated both very high waves (H_s exceeded 6 m, measured in the Firth of Forth) and surge waves exceeding 0.5 m (measured both by Aberdeen and Leith tide gauges). The waves caused significant damages to the coastal defences of cities in the SE of Scotland. In particular the City of Edinburgh council estimated the damages to coastal defences to be about GBP 23 000. Also in Berwick at the southern entrance of the Firth of Forth some damages were caused to the harbour infrastructures. To the east, in Dumbar waves topped the roof of 2-floor houses.

Damaging conditions associated with this storm were caused by a combination of simultaneous factors: (1) tides in the spring period, (2) a surge wave of about 0.5 m generated by local pressure and wind, (3) wind-sea waves generated locally that were interacting with strong currents, (4) a weak, but significant, swell waves field, interacted with the windsea waves.

3113

Figure 9 shows the intensity of the current in Aberdeen wave gauge location and the resulting wave–current interaction. In can be seen that the current was strongly enhanced by the wind, and, consequently the WCI effect was stronger.

At about 00:30 a.m. on 31 March 2010 the storm was at its maximum causing the wave field to hit the coastline at around the same time as high tide and surge. The different components of the storm were analyzed. First, the surge wave generated by the minimum of pressure above the North Sea was studied. Figure 10 shows the difference between the total water level and the water level due to tides at 02:00 UTC on 31 March 2015. The model predicted a surge wave up to 0.5 m. A comparison between the recorded water level and the model output showed that the model underestimated the surge wave by about 0.1 m. The reason of this underestimation could be because the boundary conditions for the model only included tidal water level and did not include the surge wave from outside the model. The surge wave extended from the Firth of Forth southwards: the water level in those regions was enhanced the water level by about 0.4–0.5 m. In addition to these surge conditions, the H_s of the waves at the same time were exceeding 7 m in the same areas (see Figs. 11 and 12). Figures 11 and 12 show the wave field at two different times at the storm, at 00:30 a.m., and at 02:00 a.m. respectively. The swell waves effect was very low, but contributed to the enhancement of H_s up to 0.5 m, while on the coastline the contribution of the WCI was very strong. At 02:00 UTC on 31 March 2010 (Fig. 12), when the storm reaches the coastline, WCI increased H_s by up to 2.5 m in many locations near the Firth of Forth (see Fig. 12d). Figures 11f and 12f show a high H_s swell waves at the entrance of the Firth of Forth. These were waves generated by the large storm shown in Fig. 11e, but are no longer influenced by the local wind, but are propagating outside the centre of the windsea waves to the coastline. H_s recorded by the Firth of Forth wave gauge measured a peak of significant wave height of 6.46 m at 05:00 UTC on 31 March 2015. The model matched the peak recorded in the wave gauge reasonably well, predicting higher values S of the Firth of Forth, where more damages were caused.

3114

3.4.3 The 19 June 2010 storm

The third storm that is considered in this paper was one that generated high off-shore waves conditions, with swell propagating to the coastline. This is an example of how the coupling of swell and windsea waves could lead to extreme wave conditions, with significant wave height exceeding 6 m offshore and 4–5 m on the coastline. Figure 13 shows the pressure conditions between the 18–20 June 2010. On the 17 June 2010 (not shown) a system of low pressure was generated between Greenland and Iceland. This minimum moved quickly to the Scandinavian peninsula, intensifying and remaining in the area of Sweden and Norway for 72 h. This low pressure caused strong winds in the northern North Sea and consequently the generation of waves in the area between the Norway and Scotland. This field of waves arrived at the Scottish coastline at the same time as the low pressure was generating high waves in the bulk of the North Sea, causing two trains of waves to be in the same place at the same time. This condition, known as crossing or bimodal sea, is quite common in the North Sea (Guedes Soares, 1984). The model hindcasted that the storm offshore was at its maximum near 16:00 UTC of the 19 June 2010 (Fig. 14). At 16:00 UTC on 19 June 2010 the modelled offshore, mid North Sea, windsea generated waves peaked at $H_s \sim 5$ m (Fig. 14e), whereas the swell waves were a little smaller with $H_s \sim 3$ –4 m (Fig. 14f). Further north, in the Moray Firth, the swell waves dominated with the swell having $H_s \sim 6$ m and the windsea having $H_s \sim 2$ m. The resulting predicted wave field had $H_s > 6$ m (Fig. 14b). In the Moray Firth H_s of more than 5 m was recorded. However, at this time, the coupling between currents and wave caused a decrease of the significant wave height at the coastline (Fig. 14c). In some locations H_s was reduced by more than 0.5 m (see Fig. 14c and d). 3 h later (Fig. 15), the turning tidal currents enhanced the waves by more than 1.5 m in coastal locations. Figure 3 shows that the model matches almost perfectly the water level recorded in the Moray Firth and in the Firth of Forth wave gauges at this time.

3115

4 Conclusions

In this study we presented a model capable of hindcasting surge and storms in the east coast of Scotland. The combination of spring tide, strong wind and high waves can be extremely threatening in coastal areas. The North Sea is one of the areas most affected by this forcings. Storms in North Sea can generate extremely high waves as well as rogue waves (Ponce de León and Guedes Soares, 2014).

Results indicate that wave–currents and wave–wave interactions play a fundamental role in the wave climate. The validation shows that the model performs reasonably well during both calm periods and storms for waves, and also performs well for tides and surges.

During severe storms, in particular when the low pressure was over England and Scotland, was found that the wave–current interactions (WCI) are significant, causing an increase, or decrease, in H_s that can exceed 2 m in some coastal areas, depending on the direction of the wave field compared to the current. A similar result was found for the peak spectral wave period: Fig. 4 shows that in the time period considered here the largest deviation of wave periods due to WCI is in the estuarine areas of the east coast, with average deviations more of than 1.2 s.

Wave propagation in the Firth of Forth during storms generated in the mid-North Sea is driven by trains of swell waves detaching from the open-sea storm. During the stormy periods considered here, the windsea waves in the Firth of Forth did not exceeded 3.5 m in the outer area of the estuary and 1 m in the inner part, while the swell field exceeded 5 m at the entrance of the Firth of Forth. In the inner Firth the swell waves have a similar magnitude to the windsea waves. Conversely, the area of the estuary of the Forth is mainly driven by locally generated waves. A similar behavior was noticed in the other two estuarine areas on the east coast: the Tay estuary and the Moray Firth.

The north-east coast of Scotland is more exposed to swell arriving from the North Atlantic and the Norwegian Sea, while the central and the southern part is more exposed to local windsea waves and to storms generated in the bulk of the North Sea.

3116

- Bretherton, F. P. and Garrett, C. J.: Wavetrains in inhomogeneous moving media, *P. Roy. Soc. Lond. A Mat.*, 302, 529–554, 1968. 3106
- Bryden, I. G. and Couch, S. J.: ME1 marine energy extraction: tidal resource analysis, *Renew. Energ.*, 31, 133–139, 2006. 3102
- 5 Cavaleri, L., Bertotti, L., Torrisi, L., Bitner-Gregersen, E., Serio, M., and Onorato, M.: Rogue waves in crossing seas: the Louis Majesty accident, *J. Geophys. Res.-Oceans*, 117, 1–8, 2012. 3101
- Chawla, A. and Kirby, J. T.: Experimental study of wave breaking and blocking on opposing currents, *Coast. Engin. Proc.*, 1, 759–772, 1998. 3102
- 10 Chawla, A. and Kirby, J. T.: Monochromatic and random wave breaking at blocking points, *J. Geophys. Res.-Oceans*, 107, 4–1, 2002. 3102
- Codiga, D. L.: Unified tidal analysis and prediction using the UTide Matlab functions, Graduate School of Oceanography, University of Rhode Island Narragansett, RI, 2011. 3108
- Davies, A., Sauvel, J., and Evans, J.: Computing near coastal tidal dynamics from observations and a numerical model, *Cont. Shelf. Res.*, 4, 341–366, doi:10.1016/0278-4343(85)90047-0, 15 1985. 3102
- Deardorff, J.: On the magnitude of the subgrid scale eddy coefficient, *J. Comput. Phys.*, 7, 120–133, 1971. 3105
- Dee, D., Uppala, S., Simmons, A., Berrisford, P., Poli, P., Kobayashi, S., Andrae, U., Bal-
maseda, M., Balsamo, G., Bauer, P., Bechtold, P., Beljaars, A. C. M., van de Berg, L., Bidlot,
20 J., Bormann, N., Delsol, C., Dragani, R., Fuentes, M., Geer, A. J., Haimberger, L., Healy, S. B., Hersbach, H., Hólm, E. V., Isaksen, I., Kållberg, P., Köhler, M., Matricardi, M., McNally, A. P., Monge-Sanz, B. M., Morcrette, J.-J., Park, B.-K., Peubey, C., de Rosnay, P., Tavolato, C., Thépaut, J.-N., and Vitart, F.: The ERA-Interim reanalysis: configuration and performance of the data assimilation system, *Q. J. Roy. Meteor. Soc.*, 137, 553–597, 2011. 3105, 3107, 3113
- DHI: MIKE 3 Hydrodynamics User Manual, vol. 1, 2011a. 3104
- DHI: MIKE 21 Wave Modelling User Manual, vol. 1, 2011b. 3105
- Dietrich, G.: Die natürlichen Regionen von Nord-und Ostsee auf hydrographischer Grundlage,
30 *Kieler Meeresforsch.*, 7, 35–69, 1950. 3102, 3104, 3111
- Egbert, G. D., Erofeeva, S. Y., and Ray, R. D.: Assimilation of altimetry data for nonlinear shallow-water tides: quarter-diurnal tides of the Northwest European Shelf, *Cont. Shelf. Res.*, 30, 668–679, 2010. 3105

3119

- Ferziger, J. H. and Perić, M.: *Computational Methods for Fluid Dynamics*, vol. 3, Springer, Berlin, 2002. 3103
- Flather, R.: Estimates of extreme conditions of tide and surge using a numerical model of the north-west European continental shelf, *Estuar. Coast. Shelf S.*, 24, 69–93, 1987. 3102
- 5 Guedes Soares, C.: Representation of double-peaked sea wave spectra, *Ocean Eng.*, 11, 185–207, 1984. 3101, 3115
- Hasselmann, K.: On the spectral dissipation of ocean waves due to white capping, *Bound.-Lay. Meteorol.*, 6, 107–127, 1974. 3107
- Haver, S.: A possible freak wave event measured at the Draupner jacket January 1 1995, *Rogue waves 2004*, 1–8, 2004. 3101
- 10 Hearn, C., Hunter, J., and Heron, M.: The effects of a deep channel on the wind-induced flushing of a shallow bay or harbor, *J. Geophys. Res.-Oceans*, 92, 3913–3924, 1987. 3102
- Heath, M. R., Sabatino, A. D., Serpetti, N., and O'Hara Murray, R.: Scoping the impact tidal and wave energy extraction on suspended sediment concentrations and underwater light climate, *TeraWatt Position Papers, MASTS*, 2015. 3117
- 15 Huthnance, J.: Physical oceanography of the North Sea, *Ocean and Shoreline Management*, 16, 199–231, 1991. 3102
- Janssen, P. A. E. M.: Nonlinear four-wave interaction and freak waves, *J. Phys. Oceanogr.*, 33, 863–884, 2003. 3117
- 20 Johnson, H. K. and Kofoed-Hansen, H.: Influence of bottom friction on sea surface roughness and its impact on shallow water wind wave modeling, *J. Phys. Oceanogr.*, 30, 1743–1756, 2000. 3107
- Komen, G. J., Cavaleri, L., Donelan, M., Hasselmann, K., Hasselmann, S., and Janssen, P.: *Dynamics and Modelling of Ocean Waves*, Cambridge University Press, 1996. 3105, 3106, 3107
- 25 Lilly, D.: On the application of the eddy viscosity concept in the inertial sub-range of turbulence, NCAR Manuscript No. 123, National Center for Atmospheric Research, Boulder, CO, 1966. 3105
- Longuet-Higgins, M. S. and Stewart, R. W.: Radiation stress and mass transport in gravity waves, with application to “surf beats”, *J. Fluid Mech.*, 13, 481–504, doi:10.1017/S0022112062000877, 1962. 3117
- 30 Nikuradse, J.: *Strömungsgesetze in rauhen Röhren*, Forschungsheft, Volume 361, VDI-Verlag, 33 pp., 1933. 3107

3120

Xie, L., Liu, H., and Peng, M.: The effect of wave–current interactions on the storm surge and inundation in Charleston Harbor during Hurricane Hugo 1989, *Ocean Model.*, 20, 252–269, 2008. 3102
 Young, I. R.: *Wind Generated Ocean Waves*, vol. 2, Elsevier, 1999. 3105

Table 1. Location of the validation/calibration instrumentation.

Description	Coordinates		Depth (m)	Used for
	longitude (°)	latitude (°)		
Aberdeen Tide Gauge	−2.0803	57.144	–	water level val/cal
Leith Tide Gauge	−3.1682	55.9898	–	water level validation
Buckie Tide Gauge	−2.9667	57.6667	–	water level validation
Firth of Forth buoy	−2.5038	56.1882	–	waves validation
Moray Firth buoy	−3.3331	57.9663	–	waves val/cal
Aberdeen wave rider	−2.0500	57.1608	–	waves validation
BODC 4551 RCM	−2.8000	57.7910	12	current validation
BODC 4561 RCM	−1.9680	57.2320	12	current validation
BODC 4562 RCM	−1.9680	57.2320	27	current validation
BODC 4571 RCM	−1.9020	57.2260	12	current validation
BODC 4572 RCM	−1.9020	57.2260	52	current validation
BODC 4582 RCM	−2.1500	56.9870	23	current validation
BODC 4591 RCM	−2.0980	56.9820	12	current validation
BODC 4592 RCM	−2.0980	56.9820	47	current validation

Table 4. Wave gauges validation.

	Coupled				Uncoupled			
	Bias	RMSE	<i>R</i>	SI	Bias	RMSE	<i>R</i>	SI
Firth of Forth								
H_s	-0.02 m	0.30 m	0.941	0.27	-0.01 m	0.30 m	0.939	0.27
T_m	-0.70 s	1.17 s	0.767	0.25	-0.76 s	1.24 s	0.758	0.27
Moray Firth								
H_s	-0.14 m	0.42 m	0.849	0.38	-0.15 m	0.42 m	0.848	0.39
T_m	-1.18 s	1.75 s	0.668	0.39	-1.23 s	1.83 s	0.656	0.41
Aberdeen								
H_s	-0.07 m	0.21 m	0.836	0.32	-0.07 m	0.22 m	0.831	0.32
T_m	-0.25 s	0.91 s	0.715	0.20	-0.30 s	0.97 s	0.701	0.21
Satellite								
Winter								
H_s	-0.2 m	0.4 m	-	0.25	-0.2 m	0.4 m	-	0.25
T_m	+0 s	0.8 s	-	0.15	+0 s	0.8 s	-	0.15
Spring								
H_s	-0.1 m	0.3 m	-	0.21	-0.1 m	0.3 m	-	0.21
T_m	+0.1 s	1.2 s	-	0.23	+0.1 s	1.2 s	-	0.23

3127

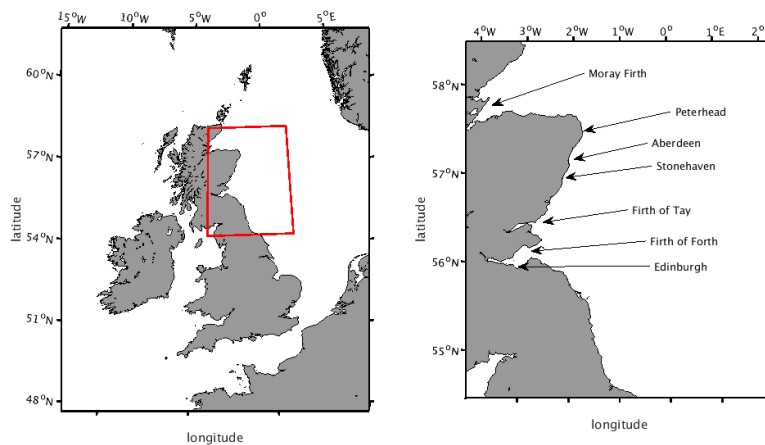


Figure 1. The area studied in the present paper.

3128

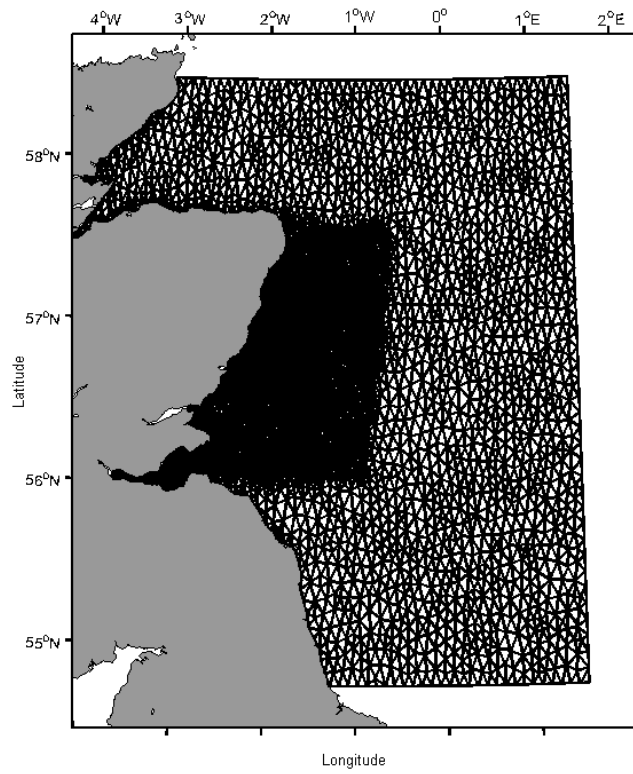


Figure 2. The computational grid generated with MIKE ZERO software.

3129

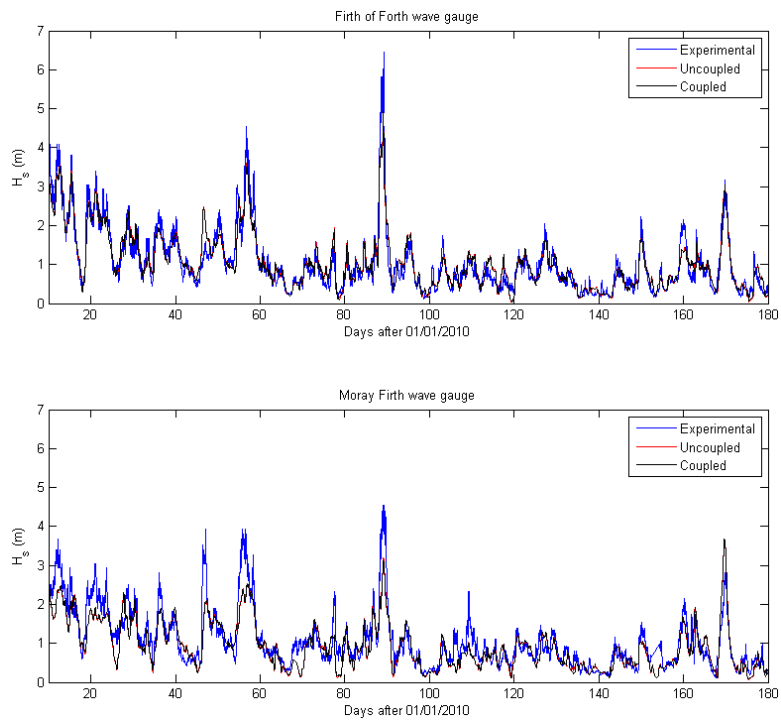


Figure 3. Comparison between experimental and modelled H_s in the Firth of Forth and in the Moray Firth for 2010.

3130

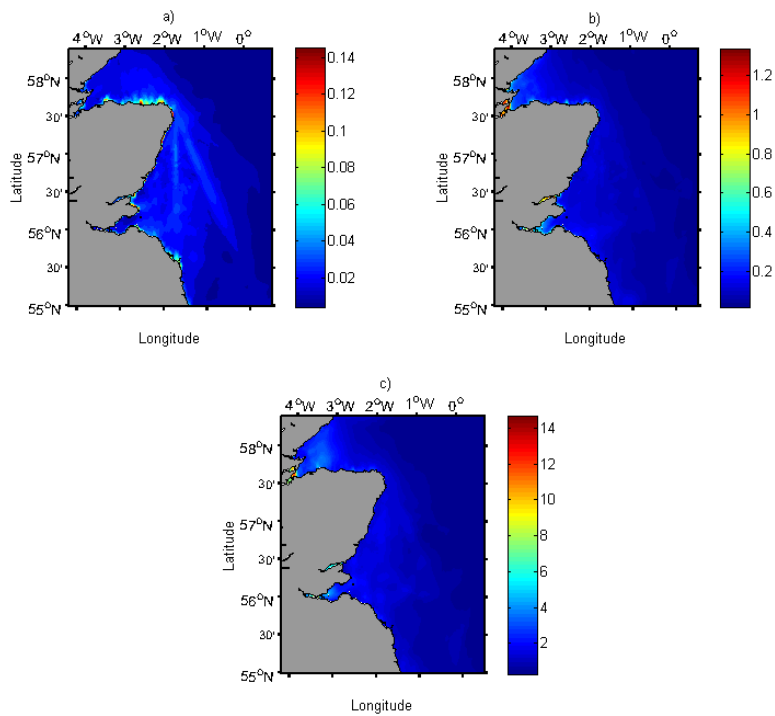


Figure 4. Root mean square difference between wave model output with and without WCI: **(a)** significant wave height (m), **(b)** peak wave period (s), **(c)** wave direction (degrees).

3131

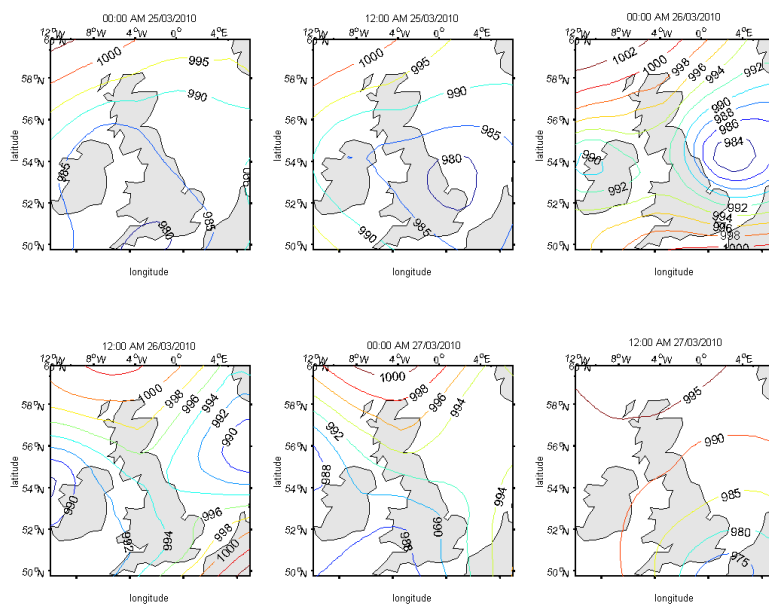


Figure 5. The mean sea level pressure fields (hPa) before and during the 25–26 February 2010 storm.

3132

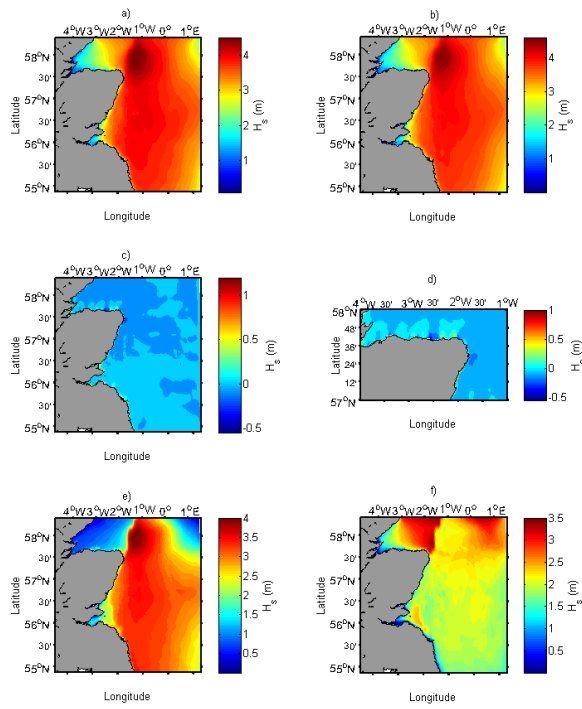


Figure 6. The modelled H_s in the east coast of Scotland at 12:30 UTC of the 26 February 2010: **(a)** coupled model (WCI on), **(b)** uncoupled model (WCI off), **(c)** difference between coupled and uncoupled, **(d)** difference between coupled and uncoupled in the Moray Firth area, **(e)** wind-sea waves, **(f)** swell waves.

3133

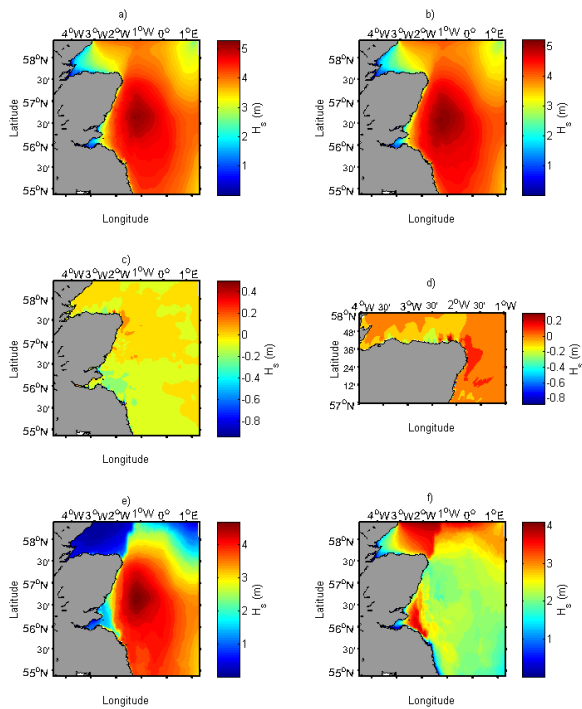


Figure 7. The modelled H_s in the east coast of Scotland at 19:00 UTC of the 26 February 2010: **(a)** coupled model (WCI on), **(b)** uncoupled model (WCI off), **(c)** difference between coupled and uncoupled, **(d)** difference between coupled and uncoupled in the Moray Firth area, **(e)** wind-sea waves, **(f)** swell waves.

3134

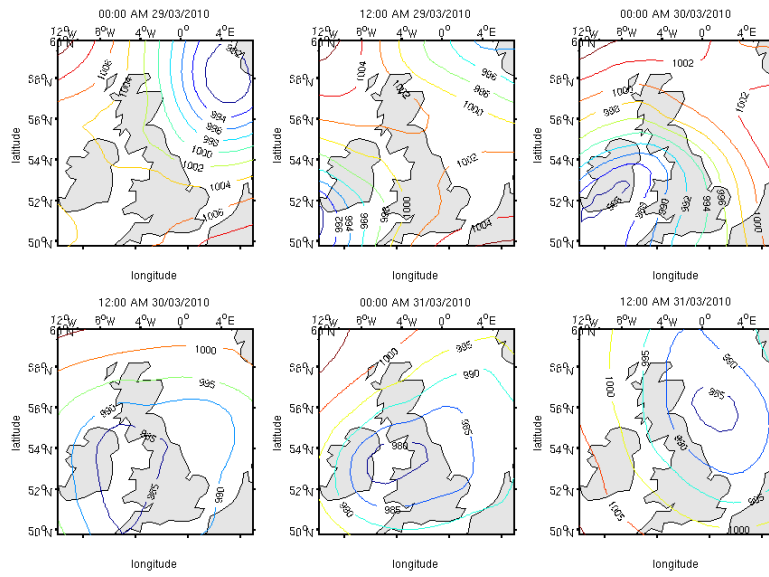


Figure 8. The mean sea level pressure fields (hPa) before and during the 30–31 March 2010 storm.

3135

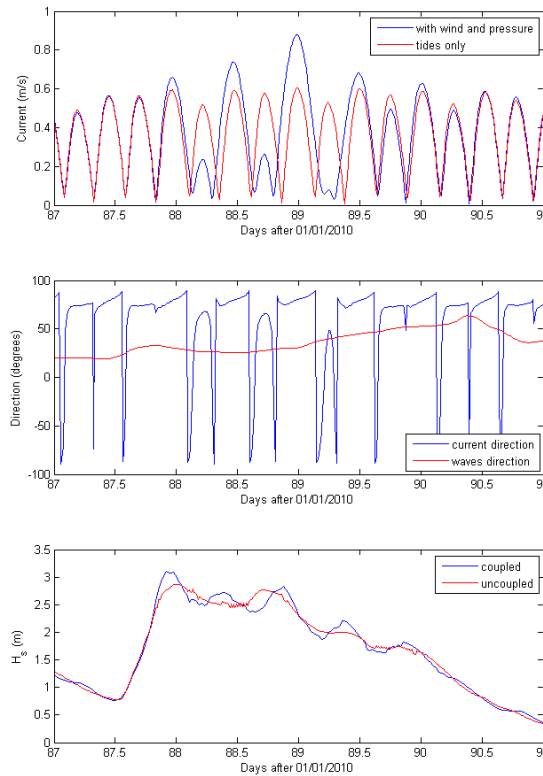


Figure 9. Modelled currents and waves conditions during the 30–31 March 2010 storm.

3136

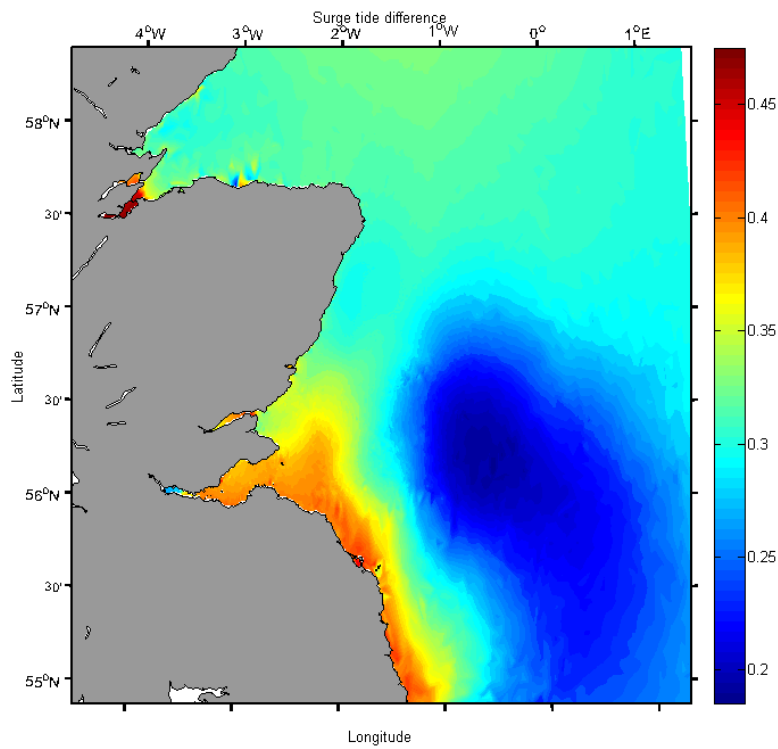


Figure 10. The surge wave at 02:00 UTC of the 31 March 2010.

3137

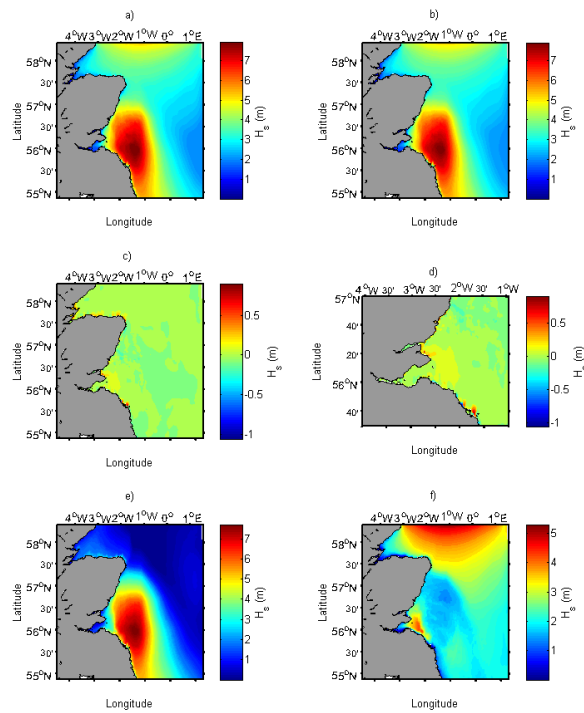


Figure 11. The modeled H_s in the east coast of Scotland at 00:30 UTC of the 31 March 2010: **(a)** coupled model (WCI on), **(b)** uncoupled model (WCI off), **(c)** difference between coupled and uncoupled, **(d)** difference between coupled and uncoupled in the Firth of Forth area, **(e)** wind-sea waves, **(f)** swell waves.

3138

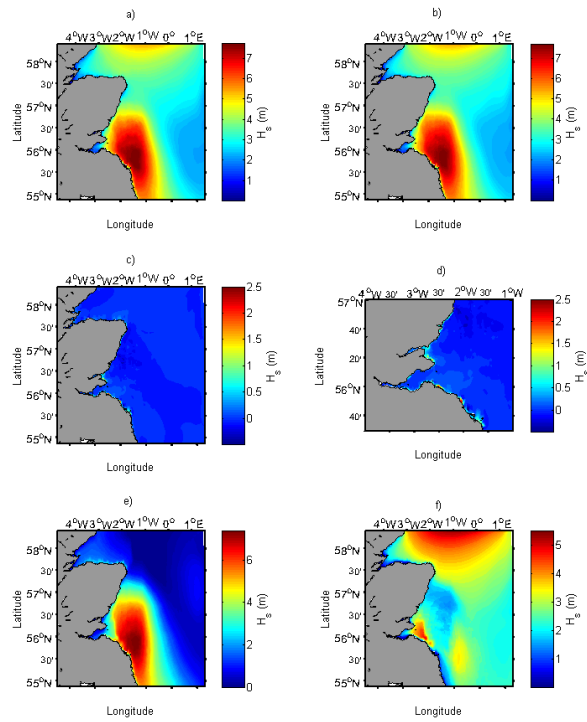


Figure 12. The modeled H_s in the east coast of Scotland at 02:00 UTC of the 31 March 2010: **(a)** coupled model (WCI on), **(b)** uncoupled model (WCI off), **(c)** difference between coupled and uncoupled, **(d)** difference between coupled and uncoupled in the Firth of Forth area, **(e)** wind-sea waves, **(f)** swell waves.

3139

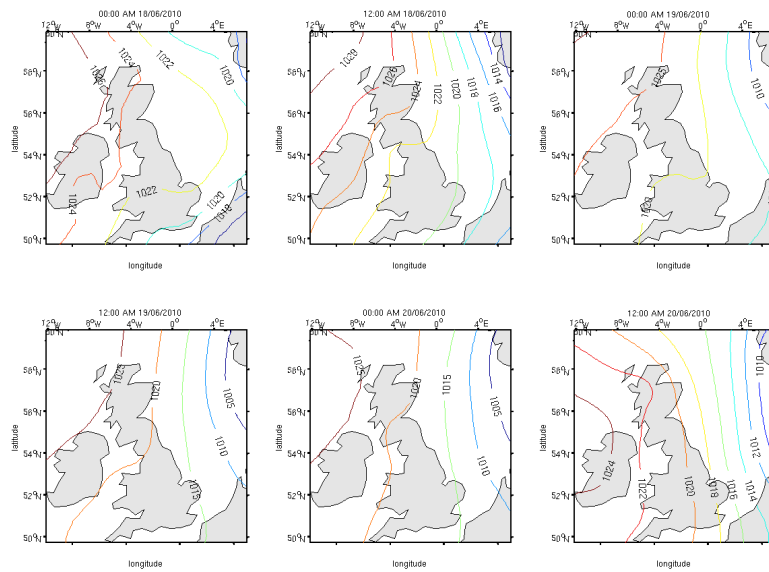


Figure 13. The mean sea level pressure fields (hPa) before and during the 19 June 2010 storm.

3140

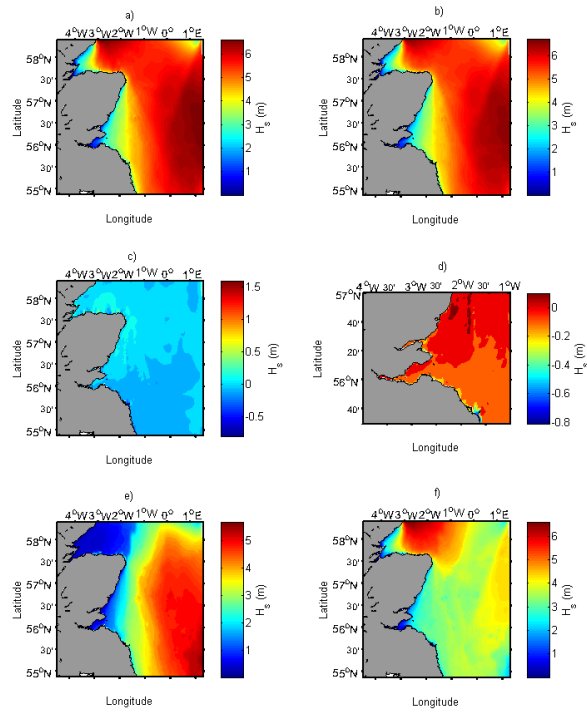


Figure 14. The modelled H_s in the east coast of Scotland at 16:00 UTC of the 19 June 2010: **(a)** coupled model (WCI on), **(b)** uncoupled model (WCI off), **(c)** difference between coupled and uncoupled, **(d)** difference between coupled and uncoupled in the Firth of Forth area, **(e)** wind-sea waves, **(f)** swell waves.

3141

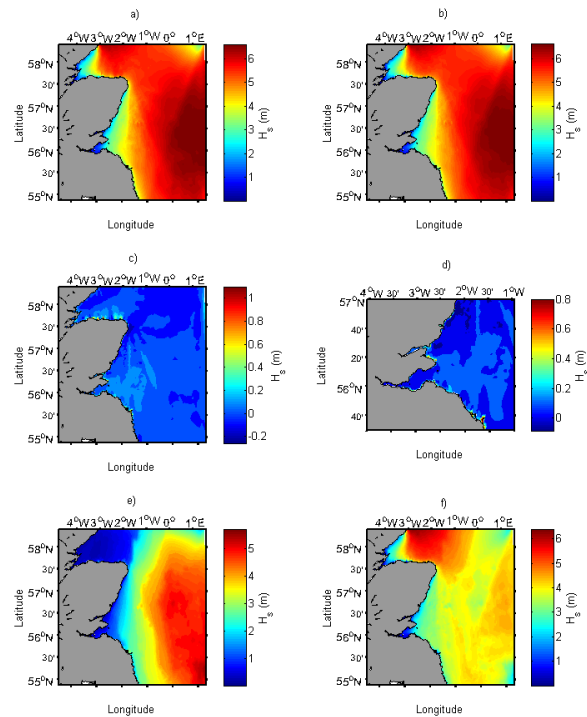


Figure 15. The modelled H_s in the east coast of Scotland at 19:00 UTC of the 19 June 2010: **(a)** coupled model (WCI on), **(b)** uncoupled model (WCI off), **(c)** difference between coupled and uncoupled, **(d)** difference between coupled and uncoupled in the Firth of Forth area, **(e)** wind-sea waves, **(f)** swell waves.

3142